High-resolution time frequency analysis using Wigner-Ville Distribution and the Maximum Entropy Method: Application for gas and hydrates identification.

Zoukaneri Ibrahim M., Milton J. Porsani CPGG/IGEO/UFBA and INCT-GP/CNPq/Brazil

Abstract

Time-frequency (TF) analysis can reveal important details of seismic data and provide valuable information for reservoir characterization. Resolution in the TF plane is clearly critical for interpretation. Many methods applied to time-frequency representation introduce spurious or cross-terms, essentially when using bilinear functions such as the Wigner Ville Distribution (WVD). Most techniques proposed to overcome this shortcoming use a smoothed kernel which in turn can adversely affect the component's concentration in the TF plane. We propose to apply the Maximum Entropy Method (MEM) to WVD to obtain a robust and high resolution time-frequency representation of seismic traces, and we also introduce a formula to estimate instantaneous frequency (IF) in time domain. We apply our approach to the spectral decomposition and IF analysis of a seismic dataset from the Gulf of Mexico. The analysis allows us to identify hydrates and a gas pocket.

Introduction

In recent years time-frequency or time-scale representations have found significant application in nonstationary analysis of a wide range of signals including seismic signals (Boashash, 1992). The position of peaks in the time-frequency representation reveals the main components or structures of the signal, and this makes it a useful tool for seismic data analysis and reservoir characterization (Wang et al., 2011). The spectrogram (Gabor, 1946), one of the earliest proposed distributions, is still commonly used to this day. However, the trade-off between temporal and spectral resolution, the so called uncertainty principle, is unavoidable. To overcome these shortcomings, other nonstationary representations have been proposed, among them are the wavelet transform, and Matching Pursuit (MP) as presented by Mallat and Zhang (1993); these techniques have been widely used in seismic signal analysis. MP suffers from high computational complexity and its time-frequency resolution depends on the dictionary, which must be carefully chosen. Other alternative representations include Cohen's class (Choi and Williams, 1989) of bilinear time-frequency energy distributions. A prominent member of this group is the Wigner-Ville distribution (WVD), which satisfies an exceptionally large number of desirable mathematical properties and exhibits the least amount of spread in the TF plane. However, because of its quadratic nature, the WVD possesses a cross component (interference term) for each pair of signal components. In practical applications, this phenomenon can reduce the readability when multi-component or nonlinear frequency modulated signals are concerned. A common strategy to reduce the impact of these cross-terms is the introduction of a fixed smoothed kernel in the WVD. Examples include the Smoothed Pseudo-Wigner Ville Distribution (SPWVD) (Franz et al., 1995), and Choi-Williams Distribution (CWD) (Choi and Williams, 1989). Other methods use an adaptive kernel such as proposed by Steeghs and Drijkoningen (2001). This method was used by Wang et al. (2011) to characterize seismic attenuation. However attenuation of the cross-terms by means of smoothing generally results in an increase of TF spread of the signal components, thus reducing the accuracy of the representation. We therefore suggest a Maximum Entropy Method (MEM) to avoid cross term representation in the WVD, by maximizing the power of each kernel of the Discrete Wigner-Ville (DWV). We compare this method to SPWVD and CWD time-frequency decomposition.

Our field data application is concerned with a problem of identification of two areas in seismic data from the Gulf of Mexico (GOM). We apply our proposed method to the analysis of the attenuation of seismic data via the method of instantaneous frequency (IF) analysis. Furthermore, we obtain the energy density distribution from the spectral decomposition of the data. This analysis allows us to identify an area of hydrates and an area of gas pocket.

Wigner-Ville Distribution and Interference terms

The Wigner-Ville Distribution (WVD) is defined as (Boashash, 1992):

$$W(t,f) = \int_{-\infty}^{\infty} x(t+\frac{\tau}{2})x^*(t-\frac{\tau}{2})e^{-2j\pi f\tau}d\tau \qquad (1)$$

where $x(t)$ is the signal, t the time, f the frequency and τ is the lag. Due to the quadratic nature of the distribution, the application of the WVD is limited by the presence of interference terms. These can be described considering elementary mono-components $z(t)$ and $g(t)$ and the WVD is then given by:

$$W_{z+g} = W_z(t,f) + W_g(t,f) + 2Re[W_{z,g}(t,f)] \qquad (2)$$

$W_z(t,f)$, and $W_g(t,f)$ are the auto-terms and $Re[W_{z,g}(t,f)]$ represents the cross-terms observed between $z(t)$ and $g(t)$ which may lead to an erroneous visual interpretation of the time-frequency representation.

Since interference terms are oscillatory they can be attenuated by means of a smoothing operation by a 2-

D smoothing kernel in the Fourier domain. This is the method adopted for Smoothed Pseudo Wigner-Ville and Choi-WIliams Distribution (Franz et al., 1995).

The Discrete Wigner-Ville Distribution

The analytic signal $z(n)$ corresponding to a signal $x(n)$ is defined in the time domain as

$$z(n) = x(n) + jH[x(n)] \tag{3}$$

where $H[x(n)]$ represents the Hilbert transform of signal $x(n)$, $n = 0,\ldots,N_s-1$, and N_s is the number of samples. The analytical signal may be used to generate a covariance matrix, $C_x = \mathbf{z}\mathbf{z}^H$. The superscript H represent the transpose conjugate of the vector $\mathbf{z}$. One may verify the hermitian property, $Real\{\mathbf{C}_z\} = Real\{\mathbf{C}_z^T\}$ and $Imag\{\mathbf{C}_z\} = -Imag\{\mathbf{C}_z^T\}$. The sequence of terms along each cross-diagonal of $\mathbf{C}_z$ is the kernel of the Discrete Wigner-Ville (DWV) distribution and may be written as,

$$K(n) = \{k_n(-l),\cdots,k_n(0),\cdots,k_n(l)\} \tag{4}$$

with terms given by,

$$k_n(l) = \begin{cases} z(n-l)z^*(n+l), & |l| \le min\{n, N_s-n\}, \\ 0, & |l| > min\{n, N_s-n\}. \end{cases} \tag{5}$$

We remark that the central term, $k_n(0)$, is associated with sample $z(n)$ of the input signal $k_n(0) = z(n)z^*(n)$.

The Fourier transform (FT) of the kernel $K(n)$ corresponds to the Wigner-Ville spectrum, which is the instantaneous power spectrum corresponding to the data point $z(n)$, and can be expressed as:

$$W(n) = \left\{ w_n(-\frac{N-1}{2}),\cdots,w_n(0),\cdots,w_n(\frac{N-1}{2}) \right\} \tag{6}$$

with coefficients given by,

$$w_n(m) = \frac{1}{N} \sum_{l=-(N-1)/2}^{(N-1)/2} k_n(l) W_4^{ml}. \tag{7}$$

N is the number of terms used in the DFT. As pointed by Bouashash (1987), equation (7) matches the standard form of a discrete FT, (DFT), except that the so called twiddle factor is normally defined as $W_2 = exp[-j2\pi/N]$. The additional power of 2 represents a scaling of the frequency axis by a factor of 2. Equation (7) can be evaluated efficiently using standard fast Fourier transform (FFT) algorithms.

The collection of instantaneous power spectrum, $W(n), n = 0,\cdots,N_s-1$, form the DWV time-frequency representation of the signal.

Properties

- The summation of kernel sequences $K(n)$ result in the sequence of even terms of the autocorrelation function (ACF) of the signal,

$$\sum_{n=0}^{N_s-1} K(n) = R_z(n), \tag{8}$$

$$R_z(n) = \{r_z(-N_s+1),\cdots,r_z(-2),r_z(0),r_z(2),\cdots,r_z(N_s-1)\}.$$

- Analogously to the marginal property of the ACF, (equation (8)), the power spectrum of the entire signal may be calculated by the summation of the instantaneous Wigner-Ville power spectrum,

$$P_z(m) = \sum_{n=0}^{N_s-1} W(n). \tag{9}$$

Others properties of DWV are discussed in Boashash (1992).

DWV in terms of the Maximum Entropy Method

We propose to use the Maximum-Entropy Method, (MEM), developed by Burg, (1975), to compute the power spectrum for every sequence of the $K(n)$, $n = 0,\ldots N_s-1$. The basic equation of the MEM is

$$P(f) = \frac{E_{N_c}\Delta t}{|1+\sum_{n=1}^{N_c} c_n e^{-j2\pi f n\Delta t}|^2}, \tag{10}$$

where $P(f)$ is the power spectrum, c_n, $n = 0,\ldots,N_c-1$, $(c_0 = 1)$, is the prediction error operator (PEO), of order N_c and E_{N_c} is its corresponding prediction error energy. f is limited by the Nyquist interval $-1/(2\Delta t) \le f \le 1/(2\Delta t)$.

The PEO can be estimated by the Levinson's algorithm or by Burg's algorithm (Burg, 1975; Levinson, 1947) from the analytical signal $z(n)$, then using directly equation (10) a time-frequency representation can be performed, nevertheless, one may like to perform the WVD because of its desirable mathematical properties, such as the marginal conditions, also we would like to derive the instantaneous frequency in time domain, so for a particular kernel $K(n)$, a corresponding trace $\widetilde{z}(n)$ is given by a window L and may be expressed as:

$$\widetilde{z}(n) = \left\{ z(n-\frac{L}{2}),\ldots,z(n),...,z(n+\frac{L}{2}) \right\} \tag{11}$$

where L is the length of the symmetric time-window, centered at $z(n)$. L is a parameter that together with the number of coefficients N_c of the PEO, controls the spectral resolution. Each coefficient of N_c can be physically associate to a plane wave. Burg's algorithm is particularly useful because, it does not impose zeros outside the window (eq. (11)), does not require previous coefficients of the ACF, and provide a minimum-phase PEO, (Ulrych and Bishop, 1975; Ulrych and Clayton, 1976; Marple, 1978; Barrodale and Erickson, 1980; Porsani, 1986).

Burg,(1975) derived the relationship between the coefficients of the ACF and the PEO, which is obtained by solving the hermitian Toeplitz system of equations. From the algorithm of Levinson (Levinson, 1947), one may write the expression which relates the PEO of order $j-1$ with the coefficients r_z of the ACF,

$$c(j,j) = \frac{r_z(j) + \sum_{i=1}^{j-1} r_z(j-i)c(j-1,i)}{E_{j-1}}, \tag{12}$$

where $c(j,j)$ is the reflection coefficient. By using equation (12) into Levinson's recursion, it can be obtained the PEO of order j from the ones of order $j-1$,

$$c(j,i) = c(j-1,i) + c(j,j)c^*(j-1,j-i) \tag{13}$$

$i = 1, \ldots, j-1$. The corresponding prediction error energy, E_j, may be updated by,

$$E_j = E_{j-1}(1 - c(j,j)c^*(j,j)). \quad (14)$$

The equations (12), (13) and (14) are essentially the kernel of the algorithm of Levinson, used to compute the PEO from the coefficients of the ACF of a given signal. The recursion start with $E_0 = r_z(0)$.

The idea is to use Burg's algorithm to provide the reflection coefficients $c(j,j)$ and Levinson's recursion in reverse order (Porsani and Ulrych, 1989), to compute and extend the terms of every Wigner-Ville kernel. Equation (12) may be rewritten as,

$$\widetilde{k}_n(j) = -\sum_{i=1}^{j-1} \widetilde{k}_n(j-i)c(j-1,i) - c(j,j)E_{j-1}. \quad (15)$$

Also, from the hermitian property of matrix $\mathbf{C}_z$, we have $\widetilde{k}_n(-j) = \widetilde{k}_n^*(j)$. The maximum-entropy instantaneous power spectrum of WVD, may be obtained by performing the DFT of the expanded kernel $\widetilde{K}(n)$, which is equivalent to use the PEO directly into equation (10).

Instantaneous Frequency estimation in time domain

The average instantaneous frequency (IF) is commonly obtained by computing the first moments of Wigner-Ville distribution (Boashash and Whitehouse, 1986), and its given by

$$IF(t) = \frac{\int_{-\infty}^{+\infty} fW(t,f)df}{\int_{-\infty}^{+\infty} W(t,f)df} \quad (16)$$

where f is frequency and $W(t,f)$ is the WVD. We propose to estimate the IF in time domain as follow: One may note that equation (16) is the inner-product between the normalized instantaneous power spectrum and the sawtooth function (Weber and Arfken, 2003). The normalization term $\int_{-\infty}^{+\infty} W(t,f)df$, in the denominator, is the time marginal of WVD and it is equal to $k_n(0)$. By using Parseval's theorems and symmetry properties of the signals, we may rewrite equation (16), in the discrete form, as

$$f(n) = \frac{2\sum_{l=1}^{l=(N-1)/2} q(l)\widehat{k}_n(l)}{Nk_n(0)} \times \frac{1}{N\Delta t} \quad (17)$$

where $q(l)$ are the coefficients of the imaginary part of the inverse FT of the sawtooth function and $\widehat{k}_n(l) = Imag(\widetilde{k}_n(l))$ are the imaginary part of the terms of the kernel $\widetilde{K}(n)$, obtained using equation (15). The term $1/N\Delta t$ is necessary to convert to frequency units.

Algorithm for WVD, or for IF directly in time domain

- Obtain the complex trace $z(n) = x(n) + jH[x(n)]$.
- Set N_c, for the number of coefficients of the PEO.
- Set L, for the window length to compute the PEO.

For $n = 0, N_s - 1$

- set $E_0 = k_n(0)$,
- collect data associated with kernel $K(n)$, (equation (11)),
- compute $c(j,j), j = 1, \ldots, N_c - 1$, using the Burg's algorithm,
- use equations (15), (13) and (14), $j = 1, \ldots, N-1$ to compute the extended DWV kernel, $\widetilde{K}(n)$,
- compute the DFT of $\widetilde{K}(n)$, to obtain the instantaneous power spectrum, (equation (6)).
- if only the IF is desired, ignore the previous step and use directly equation (17).

Figure1 shows a time-frequency distribution of a 1-D synthetic signal which include two crossing chirps using the WVD, the SPWVD, the CWD and the MEM; the proposed method recovers the nonstationary tendency with high resolution in time and frequency scale without any spurious terms, comparing to others methods. The proposed method can be further used for multicomponent or well-seismic data registration (Fomel and Backus 2003, Fomel et al, 2005). In the synthetic case, the coefficient number $N_c = 5$ was used. A high number of coefficients may be used in practical application for components separation. In the real case showed in Figure 2, $N_c = 2$ was enough to insure a high resolution representation. the spectrum obtained with $N_c = 2$ can be traduce as an average spectrum obtained by propagating infinitely one plane wave. The effect of the window length is showed in Figure 3 with the IF curve overlain. As soon as the window decrease the time-frequency resolution increase. We remark that, for a fixed L, the IF curve does not change significantly when varying the number of coefficients Nc, meaning that the method is robust and provide a stable estimation of the IF.

Application to GOM data

In Figure 4 we have a section of GOM data where areas of high energy reflectors can be observed in the shallow part (area 1 and 2). Initially, it is not possible to associate both areas to the same event, such as the presence of gas or hydrates, or to a strong lithology contrast. It can also be observed that there is an amplitude dimming in the structures at depth. To identify those areas we based our analysis on attenuation characterization and energy density distribution.

Figure 5, shows the instantaneous frequency image of the seismic data which serves as measure of the attenuation effect. Three zones are defined: HFZ (High Frequency Zone around 30 Hz), MFZ (Median Frequency Zone around 15 Hz) and LFZ (Low Frequency Zone around 5 Hz). Areas 1 and 2 show high frequency content. Below area 1, we observe a median frequency zone (MFZ), whereas below area 2 we have a low frequency zone (LFZ), both areas caused attenuation, but the attenuation effect caused by area 1 is lower than the one caused by area 2. On the other hand, the LFZ observed below area 1 can not be directly related to the effect of that area, so we perform the spectral decomposition to complete the analysis. Figure 6 shows the energy density at 5 Hz where it can be observed the so called low frequency shadow which is commonly used as direct hydrocarbon indicator (Castagna et al., 2003, Wang, 2007, Oliveira et al., 2010), and it is generally interpreted as caused by attenuation. Nevertheless this phenomenon can be also related to velocity effect or thin bed effect as pointed by Shenghon et al., (2009), and Wang (2010). Interpreting the low frequency shadow as an indicator of hydrocarbon, we associate the amplitude dimming of the zone LFZ below area 1 to be caused by the presence of a reservoir, and not related to area 1.

Figure 7 shows RGB blending applied following the spectral decomposition where the shape and extend of both areas can be clearly observed; both areas show high energy density, but each one is associate to different frequencies; area 1 contains lower frequency energy (15 Hz) than area 2 (30 Hz). We conclude that the two areas are not from

the same event. Complementary velocity analysis (not show here) confirmed that area 1 has higher velocity than area 2. This suggest that area 1 can be associated with the presence of hydrates and area 2 with a gas pocket. The gas pocket may be causing the observed amplitude dimming in zone LFZ directly below it.

In summary, then, the combined analysis of this set of data using instantaneous frequency analysis and spectral decomposition, indicates that area 1 and 2 are of high energy density, high frequency content, and caused attenuation on structures below, then can be considered as absorption zones. In addition, the area 1 has lower frequency than area 2, as well the attenuation effect caused by area 1 is lower. This analysis confirm the difference between both areas and allows to concluded that area 1 is likely related to the presence of hydrates and area 2 to a gas pocket.

Conclusion

A high resolution time-frequency representation of seismic data has been presented using a new approach based on Wigner-Ville Distribution and Maximum Entropy Method. It has been also introduced a new equation to compute the instantaneous frequency directly in time domain. The application on field data allows a reliable analysis of attenuation effect and energy density distribution, through the instantaneous frequency and spectral decomposition analysis, it has been identified the hydrates from gas pocket area, as well as the shape and extend of both zones.

Acknowledgements

The authors want to thank PEMEX for the kindness in authorizing the data, INCT-GP/CNPq for the support and CGG for permitting to publish this work. We thank Gulunay Necati and Hoeber Henning for they suggestions.

References

Barrodale, I. and R. E. Erickson, 1980, Algorithm for least-squares linear prediction and maximum entropy spectral analysis - Part I: Theory: Geophysics, **45**, 420–432.

Boashash, B., 1992, Estimating and interpreting the instantaneous frequency of a signal: Part 1. Fundamentals: Proc. IEEE, **80**, 519–538.

Boashash, B. and H. J. Whitehouse, 1986, Seismic applications of the Wigner-Ville Distribution: IEEE, 34–37.

Bouashash, B., 1987, An efficient real-time implementation of the Wigner-Ville Distribution: IEEE Transactions on Acoustics, Speech, and SP, **35**, 1611–1618.

Burg, J. P., 1975, Maximum entropy spectrum analysis: Phd. dissertation. Dep. Geophysics Stanford University, CA, USA.

Castagna, J. P., S. J. Sun, and R. W. Siegfried, 2003, Instantaneous spectral analysis: Detection of low-frequency shadows associated with hydrocarbons: The Leading Edge, **22**, 124–127.

Choi, H. I. and W. J. Williams, 1989, Improved time-frequency representation of multicompnent signals using exponential kernels: IEEE trans. Acoust. Speech Signal Process, **ASSP-37**, 862–871.

Franz, H., T. G. Manickam, R. L. Urbanke, and W. Jones, 1995, Smoothed pseudo-wigner distribution Choi-Williams distribution, and Cone-kernel representation: Ambiguity analysis and experiemental comparision: Elsevier, Signal Processing, **43**, 149–168.

Gabor, D., 1946, Theory of communication: Journal of the Institute of Electrical Engineers, **93**, 429–457.

Levinson, N., 1947, The Wiener RMS (Root Mean Square) criterion in filter design and prediction: J. Math. Phys., **25**, 261–278.

Mallat, S. G. and Z. Zhang, 1993, Maching pursuit in a time-frequency dictionary: IEEE Transactions on Signal Processing, **41**, 3397–3415.

Marple, S. L., 1978, Frequency resolution of high resolution spectrum analysis technique: in Proc. 1st RADC spectrum estimation workshop, 19–35.

Oliveira, O., O. Vilhena, and E. Costa, 2010, Time-frequency spectral signature of pelotas basin deep water gas hydrates system: Mar Geophy Res, **31**, 89–97.

Porsani, M. J., 1986, Desenvolvimento de algoritmos tipo-Levinson para o processamento de dados sismicos: Phd disserttion, Universidade Federal da Bahia, Salvador, Brasil www.pggeofisica.ufba.br/publicacoes/detalhe/205.

Porsani, M. J. and T. J. Ulrych, 1989, Discrete convolution by means of forward and backward modeling: IEEE, transaction on acoustic, speech and signal processing, **37**, 1680–1687.

Shenghong, T., C. P. Jons, and J. P. Castagna, 2009, Local frequency as a direct hydrocarbon indicator: SEG extended abstract.

Steeghs, P. and G. Drijkoningen, 2001, Seismic sequence analysis and attribute extraction using quadratic time-frequency representations: Geophysics, **66**, 1947–1959.

Ulrych, T. J. and T. N. Bishop, 1975, Maximum entropy spectral analysis and autoregressive decomposition: Rev. Geophys., **13**, 183–200.

Ulrych, T. J. and R. W. Clayton, 1976, Time series modelling and maximum entropy: Phys. Earth Planet. Int., **12**, 188–200.

Wang, X., G. Jinghuai, C. Wenchao, X. Jin, W. Z, and J. Xiudi, 2011, Adaptive optimal-kernel time-frequency representation and its application in characterizing seismic attenuation: SEG extended abstract.

Wang, Y., 2007, Seismic time-frequency spectral decomposition by matching pursuit: Geophysics, **72**.

———, 2010, Reservoir characterization based on spectral variations: Geophisics, **77**, 89–95.

Weber, H. J. and G. B. Arfken, 2003, Essential mathematical methods for physicists: Academic Press.

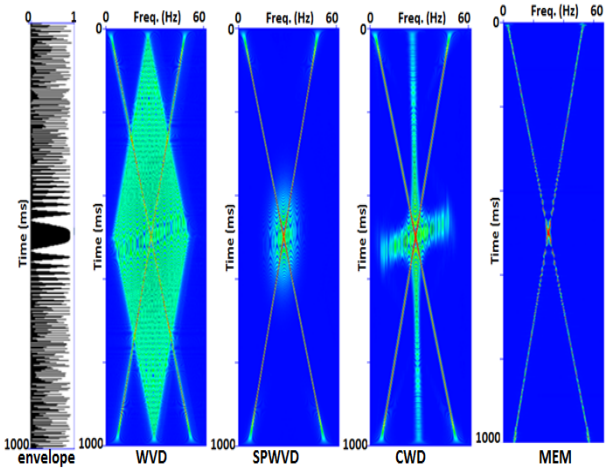

Figure 1: Comparison of methods using synthetic data.

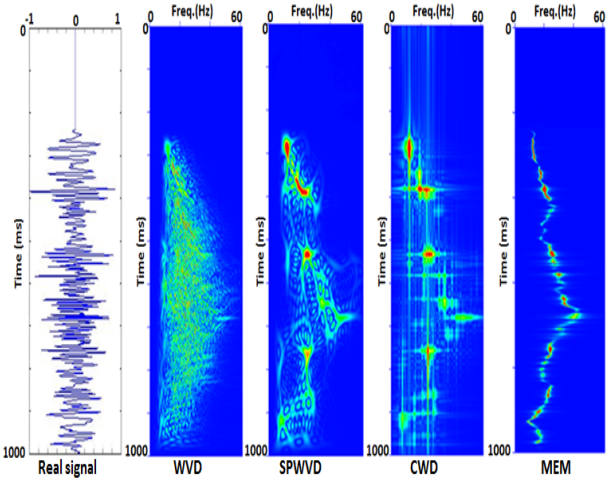

Figure 2: Comparison of methods using real data.

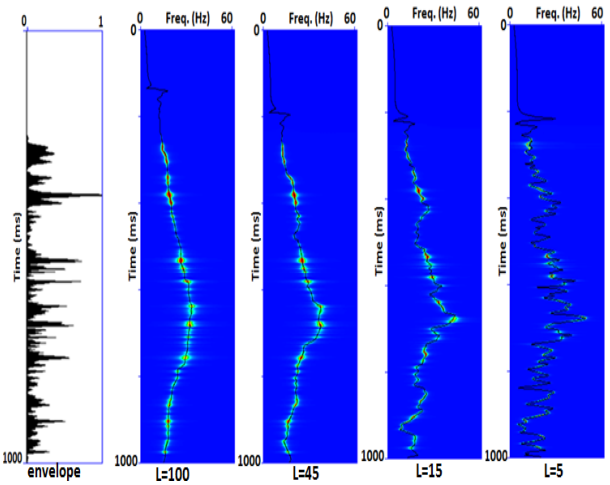

Figure 3: Effect of the window length (L), and the IF overlain, obtained using equation (17).

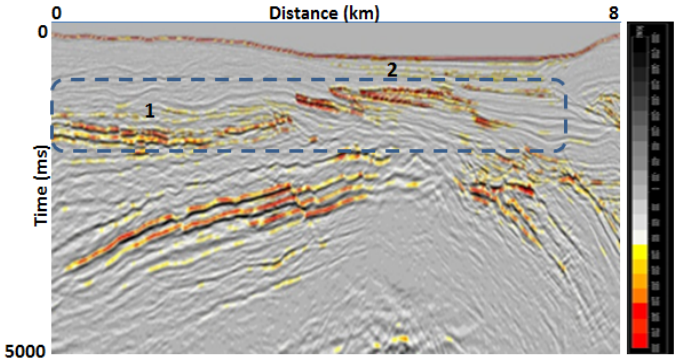

Figure 4: Seismic data.

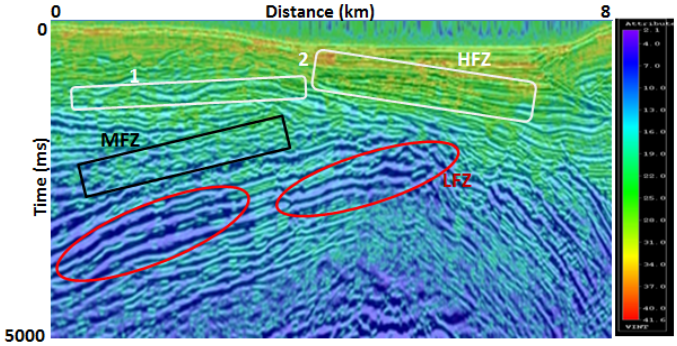

Figure 5: Instantaneous frequency of real GOM data, HFZ= High frequency Zone, MFZ=Median frequency Zone, LFZ= Low frequency zone.

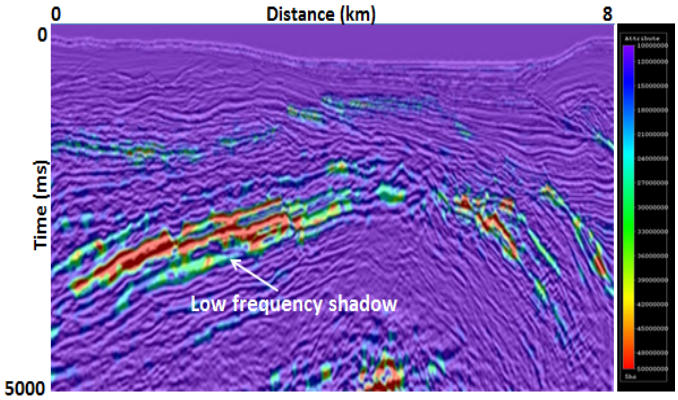

Figure 6: Energy density.

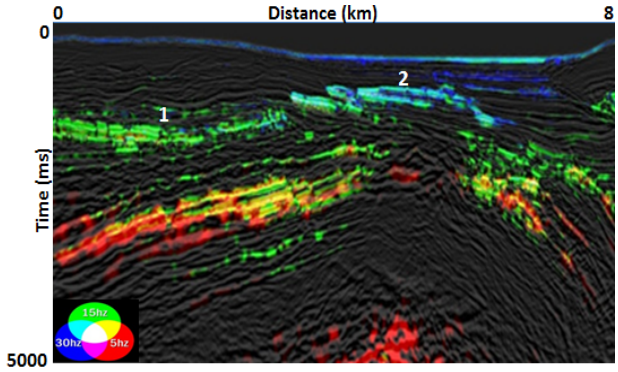

Figure 7: RGB blending using 5Hz, 15Hz and 30 Hz spectra.